Construction and Building Materials 335 (2022) 127523

Contents lists available at ScienceDirect

Construction and Building Materials

journal homepage: www.elsevier.com/locate/conbuildmat

Grid nanoindentation on calcium sulfoaluminate (CSA)-Kaolinite pastes

Umme Zakira [a,*], Aayushi Bajpayee [b], Matt Pharr [c], Sarbajit Banerjee [d], Bjorn Birgisson [e]

[a] Zachry Department of Civil and Environmental Engineering, Texas A&M University, College Station, Texas, TX 77843-3136, USA
[b] Department of Chemistry, Department of Material Science and Engineering, Texas A&M University, College Station, Texas, TX 77842-3012, USA
[c] Department of Mechanical Engineering, Texas A&M University, College Station, Texas, TX 77843-3123, USA
[d] Department of Chemistry, Department of Material Science and Engineering, Texas A&M University, College Station, TX 77842-3012, USA
[e] Zachry Department of Civil and Environmental Engineering, Texas A&M University, College Station, TX 77843-3136, USA

ARTICLE INFO

Keywords:
Calcium sulfoaluminate cement (CSA)
Kaolinite
Grid nanoindentation
Elastic modulus
Hardness
Roughness RMS
Histogram
Probability density function (PDF)
Ettringite
Statistical analysis

ABSTRACT

Calcium sulfoaluminate cement (CSA) has garnered attention in the construction industry as a low carbon footprint binder. CSA-kaolinite is a potential building material of the future and holds promise as a sustainable cement-based concrete. While the macroscopic properties of CSA cement have been extensively investigated, the nanomechanical properties of CSA-kaolinite remain largely underexplored. This study investigates the nanomechanical properties (elastic modulus and hardness) of CSA-kaolinite samples by using a grid nanoindentation approach, which enables both spatial mapping and indentation depth studies. A frequency-histogram-derived probability density function (PDF) model was found to fit well to the experimental dataset and revealed that the dominant phase of the system is ettringite irrespective of incorporation of kaolinite. The elastic modulus of ettringite was determined to be 20.8 and 17.5 GPa for samples without and with kaolinite, respectively, which is consistent with results from previous studies. Furthermore, a microstructural investigation confirmed ettringite as the major hydration phase of the system. Descriptive statistics, t-tests, and Kruskal–Wallis analysis of variance (ANOVA) were performed to determine if the measurements belong to a different group of populations. Non-parametric tests were found to be more accurate for these highly heterogeneous and skewed groups of cement-based materials. The mechanical properties from the samples of CSA with kaolinite and from those without kaolinite were found to be significantly statistically different which demonstrates that the nanoindentation test results are from two different sets of samples. The addition of kaolinite, as much as 10 wt%, in the CSA system has a trivial effect on the microscale mechanical properties which broadens the perspective of utilizing the kaolinite as a building constituent prolonging the advantages of infusing sustainability in the construction industry.

1. Introduction

Calcium sulfoaluminate cement (CSA) has been recognized as a 'Low-Energy Cement' [6] and affords outstanding material properties such as fast setting, high early strength, good durability, and corrosion resistance depending on the clinker formulations [30]. The utilization of naturally occurring clays enables mesoscale tailoring of sustainable construction material [1]. The *in situ* incorporation of kaolinite in CSA cement represents an attractive alternative for the development of sustainable low-carbon-footprint building materials. Several studies have focused on the microstructural investigation and mechanical characterization of the CSA cement system at the micro-scale [11,27,28,32]. However, nanoscale studies on the CSA cement system are limited. In one such study, [11] performed mechanical characterization of a CSA cement-gypsum blend using nanoindentation and correlated with microstructural properties. They identified six different microstructures based on indentation modulus and hardness: one with more ettringite, one with less ettringite and more aluminum hydroxide, and other microstructures of belite, ye'elimite, and the interface between the hydration product and unhydrated cement. The microstructure with more ettringite showed lower mechanical properties, indentation modulus of 22.9 ± 3.9 GPa and hardness of 0.77 ± 0.14 GPa, than the hydration phase with lesser ettringite, indentation modulus of 28.4 ± 4.5 GPa, and hardness of 1.13 ± 0.21 GPa. Still, studies that use nanoindentation on

* Corresponding author.
E-mail addresses: uz17@tamu.edu (U. Zakira), a.bajpayee@tamu.edu (A. Bajpayee), mpharr85@tamu.edu (M. Pharr), banerjee@chem.tamu.edu (S. Banerjee), bjorn.birgisson@tamu.edu (B. Birgisson).

https://doi.org/10.1016/j.conbuildmat.2022.127523
Received 25 January 2022; Received in revised form 10 March 2022; Accepted 12 April 2022
Available online 18 April 2022
0950-0618/

pure CSA cement and systems of CSA with kaolinite are limited. Integrating kaolinite in CSA would extend the utilization of widely available materials in infrastructure material innovation. Therefore, nanomechanical studies of CSA cement incorporating kaolinite is imperative to decipher the mechanistic basis for early strength and to develop strategies for optimal hydration across length scales. A detailed nanomechanical mapping in tandem with careful surface preparation, as well as statistical and microstructural analysis of CSA cement with kaolinite needs to be explored to understand the effect of kaolinite on the micromechanical properties of CSA-based systems.

Nanoindentation has been adopted as an effective small-scale mechanical characterization tool for the last few decades [7,10,12,15,17,18,22,26]. The ubiquitous implementation of the method has enabled the investigation of cement-based materials across length scales from nanometer-sized to micron-sized dimensions. Characterization of cement-based matrices is complex because of the heterogeneity of the system, yet crucial for mesoscale tailoring of the material to achieve optimal performance as a building material. Several studies have been conducted on the microstructural mechanical performance of cementitious materials [2,3,5;13,14,16,20,31]. The grid nanoindentation technique is advantageous for multiphase and heterogeneous materials where nanoindentation is performed on each point of a large grid of sample area. The spacing between the grid points can be from 3 μm to 10 μm to avoid the influence of the particle size [2]. In combination with nanoindentation mapping, microstructural characterization and statistical analysis such as probability density function (PDF) and cumulative distribution function (CDF), different phases and their mechanical properties can further be determined [16,24,29,33]. The choice of indentation depth plays a vital role to ensure self-similar material properties which, for cement-based materials, depends on the size of the hydration phases. The appropriate indentation depth for cement-based materials ranges from 100 nm to 1000 nm (Hu & Li, 2015c) [33] and a maximum of 1500 nm [14]. One of the major challenges in nanoindentation tests is to ensure good surface preparation such as to minimize surface roughness. Adequate surface preparation can be validated by atomic force microscopy (AFM) measurements of the root mean square roughness (RMS), which should be 5 times lower than the indentation depth for the specific scan size [19]. Statistical analyses aid interpretation of the mechanical properties of each phase present as well as the dominant segment, if any, within the system. A common practice in a statistical-based nanoindentation technique, especially in multiphase systems, is approximation of mechanical properties of each phase by assuming Gaussian distributions to best fit the experimental results using a nonlinear least square method (Hu & Li, 2015c).

The present work aims to evaluate the nanomechanical properties of the CSA cement system along with the effect of incorporation of kaolinite on structural performance. Detailed nanomechanical and indentation mapping was performed. Grid nanoindentation in combination with atomic force microscopy (AFM) and statistical analysis were performed on 28-day hydrated CSA cement paste with and without kaolinite along with microstructural investigation using X-ray diffraction (XRD) and scanning electron microscopy (SEM). Descriptive statistics, a two-sample *t*-test, and Kruskal–Wallis analysis of variance (ANOVA) were used to determine the differences between these two datasets. The RMS roughness was used to evaluate the surface preparation of the thin sections used in the nanoindentation test.

2. Materials and methods

2.1. Materials and sample preparation

Two sets of samples were prepared to contain calcium sulfoaluminate (CSA) cement ($d_{50} < 11.89$ μm) with (denoted as CK) and without (denoted as C) kaolinite ($d_{50} < 4.5$ μm) with a cement-to-kaolinite weight ratio of 2.67 (equivalent to 10 wt% of the dry ingredients). The CSA contains 49.6% ye'elimite, 29.9% larnite (belite), 17% soluble anhydrite, and 3.5% calcite. The weight ratio of water to binder was kept constant as 0.45. The fresh cement pastes were mixed according to ASTM C305 and poured into a 2"×1" cylindrical mold after manual compaction. The samples were de-molded after 24 h, followed by cured at room temperature under 95% relative humidity for 28 days.

For the nanoindentation tests, the 28-day cured cement pastes were immersed into ethanol for 30 min to stop the hydration reaction. A geological cutting machine was used for sectioning the specimen for the test. Thin sections of 25 mm × 50 mm × 0.025 mm were prepared by cutting slices with a diamond saw followed by mounting on a glass slide, and then grinding and polishing with a microprobe down to a thickness of 25 μm. An optical microscope was used after each step to check the effectiveness of grinding and polishing. The sections were prepared with epoxy resin impregnation to fill the voids and to avoid damage to microstructure during polishing and cutting. An oil-based liquid was used as a lubricant during microprobe polishing to protect the samples from further hydration.

2.2. Nanoindentation methods

Quasistatic grid nanoindentation was performed using a TI 950 Triboindenter with a 10 to 15 mN standard load transducer and a diamond Berkovich tip. The tip was calibrated each time with a fused silica standard of known mechanical properties and area function [23]. A 1000 nm displacement control approach was chosen in conjunction with a loading pattern of 10 s of loading, followed by a 5-second hold at the maximum load to reach the maximum displacement, and then followed by 10 s of unloading (Fig. 1b).

The indentation depth was chosen to be 1000 nm for the ease of indent identification and imaging [33]. The nanoindentation was performed with displacement control setup, all indents except a few indents could not reach 1000 nm due to reaching maximum capacity of the load cell. A 14 × 14 grid indentation summing to 196 indentations on each sample was performed with a spacing of 10 μm between each grid point as shown in Fig. 1a. Fig. 1 (d-e) shows the optical microscopic images of the 14 × 14 grid indentation of 196 indents on samples 'C' (CSA cement paste) and 'CK' (CSA and kaolinite paste).

The indentation load–displacement data for a Berkovich indenter was evaluated according to Oliver-Pharr methodology [22] to obtain the elastic properties. The reduced elastic modulus represents the elastic deformation that occurs in both the sample and the indenter tip. The reduced modulus, E_r is defined by:

$$E_r = \frac{\sqrt{\pi}}{2}\frac{S}{\sqrt{A_C}} \tag{1}$$

And the indentation hardness, H:

$$H = \frac{P}{A_C} \tag{2}$$

Where S is the initial slope of the unloading portion of the load–displacement (P-h) curve (Fig. 1c), P is the indentation load, and A_C is the projected contact area of the indenter at peak load. The modulus of the specimen can be calculated from reduced modulus which also accounts for the effect of the non-rigid indenter with the following equation:

$$\frac{1}{E_r} = \frac{1-\nu^2}{E} + \frac{1-\nu'^2}{E'} \tag{3}$$

Where E_r is reduced modulus (measured), E is the modulus of the specimen, E' is the modulus of the indenter (1140 GPa), ν' is the Poisson's ratio of the indenter (0.07), and ν is the Poisson's ratio of the specimen = 0.3 (assumed).

The topographic data was obtained by performing atomic force microscopy (AFM) on the indentation area with a Dimension Icon micro-

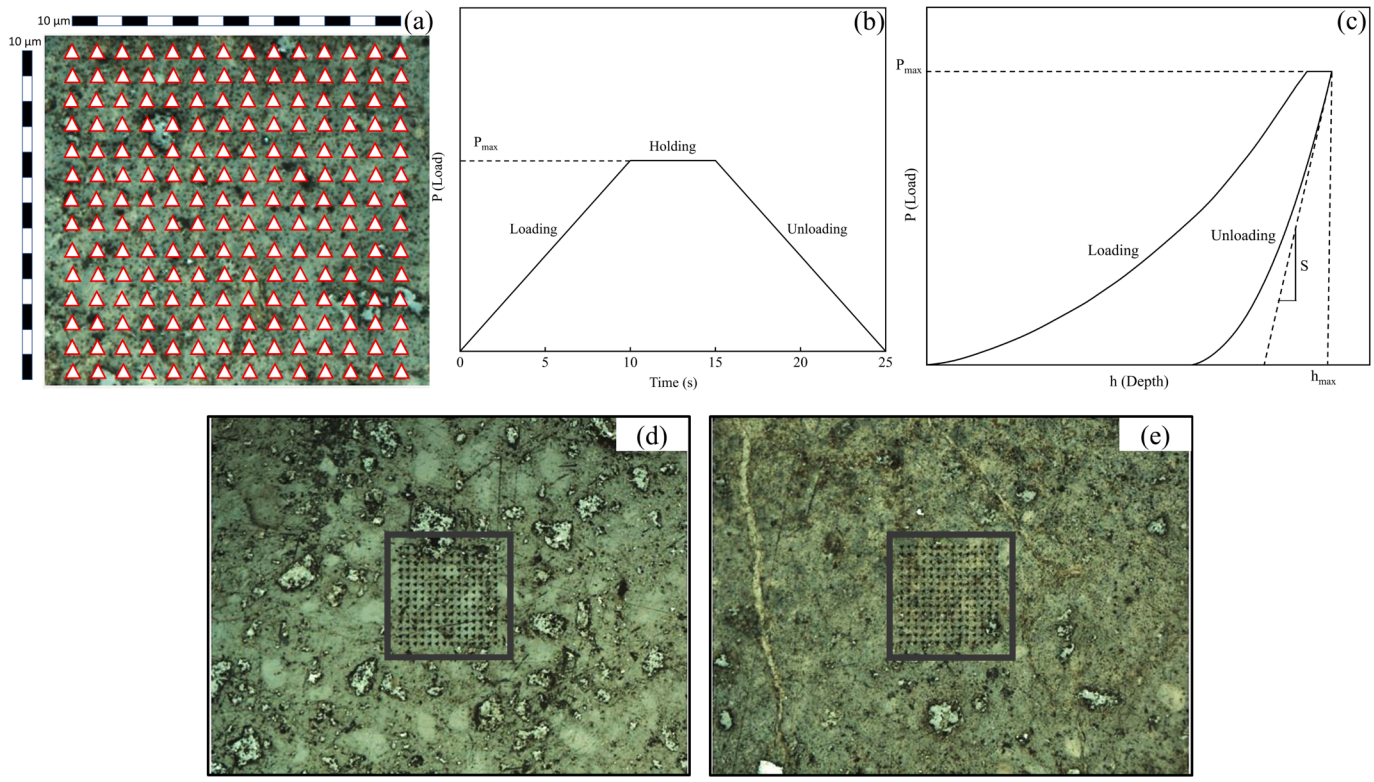

Fig. 1. Schematic of (a) grid nanoindentation plan on an optical image of a CSA with kaolinite (CK) sample, (b) loading pattern for displacement control setup, (c) typical load vs. indenter depth curve for the study, (d) Optical microscopy image after performing grid indentation on a sample of CSA cement paste (C) and (e) CSA cement paste with kaolinite (CK).

scope. Topographic images were taken using Peak Force Quantitative NanoMechanics (PF-QNM) imaging mode with a rectangular 0.01–0.025 Ω-cm antimony (n) doped silicon probe having a cantilever thickness of 5.75 μm and a spring constant of 200 N/m. The scan size, scan rate, and image resolution were 60 × 60 μm, 0.5 Hz, and 512 × 512 pixels, respectively. The topographic images were further analyzed for determining the root-mean-squared average (RMS) surface roughness (R_q), defined by:

$$R_q = \sqrt{\frac{1}{N^2}\sum_{i=1}^{N}\sum_{j=1}^{N} z_{ij}^2} \tag{4}$$

where N is the number of pixels in each scan edge and z_{ij} is the height at position (i, j) from the mean plane. The scan lengths were 10 × 10 μm, 15 × 15 μm, and 20 × 20 μm for both the cement paste with (denoted as CK) and without kaolinite (denoted as C). An average of three estimations was reported for each scan size.

The morphologies of the kaolinite-infused calcium sulfoaluminate cement composite were imaged using a JEOL JSM-7500F field-emission scanning electron microscope (SEM) operated at an accelerating voltage of 5 kV. Phase identification of hydration products for the kaolinite-infused calcium sulfoaluminate cement composite was achieved by powder X-ray diffraction (XRD) using a Bruker-AXS D8 Vario diffractometer with a Cu Kα (λ = 1.5418 Å) radiation source.

2.3. Statistical analysis

Each data set of mechanical properties was presented with a histogram with a chosen bin size of 0.3 GPa for reduced modulus and 0.02 GPa for hardness. The probability density function (PDF) was calculated based on the assumption that the mechanical properties of each phase follow a Gaussian distribution and the measured data were analyzed to fit using the nonlinear least square method. Based on these assumptions the PDF of each phase can be expressed as:

$$P_i(H) = \frac{1}{\sqrt{2\pi{\sigma_i}^2}}\exp\left(\frac{-(x-\mu_i)^2}{2{\sigma_i}^2}\right) \tag{5}$$

In each model fit, μ is the mean value, and σ is the standard deviation of the distribution.

A separate variance test was executed between CSA with kaolinite and without kaolinite datasets to determine the difference between the distributions. A nonparametric variance test, Kruskal–Wallis analysis of variance (ANOVA) was used to determine if the two sets of data are from significantly different samples. The Kruskal–Wallis test statistic, H′, can be defined by:

$$H' = \frac{12}{N(N+1)}\sum_{i=1}^{k}\frac{{R_i}^2}{l_i} - 3(N+1),\ N = \sum_{i=1}^{k} l_i \tag{6}$$

Where N is the number of observations and (k-1) is the degree of freedom. From the ascending ordered dataset, the average ranks, R_i, are assigned to tied scores summing to up to k. In case of tied scores, the H' is corrected by dividing $\left(1-\frac{\sum(t^3-t)}{N^3-N}\right)$, where, t is the number of tied scores in a group, and the summation is over all tied groups. The analysis is based on the null hypothesis that the median of the two distributions is equal (two samples came from the same population). The Kruskal–Wallis statistic also approximates a probability value. If the probability value (p) is less than the significance level (α = 0.05), the null hypothesis will be rejected.

3. Results and discussion

3.1. AFM imaging and roughness analysis

Fig. 2 (a and b) shows the topographic images of residual imprints of the indents on samples 'C' (CSA cement paste) and 'CK' (CSA with

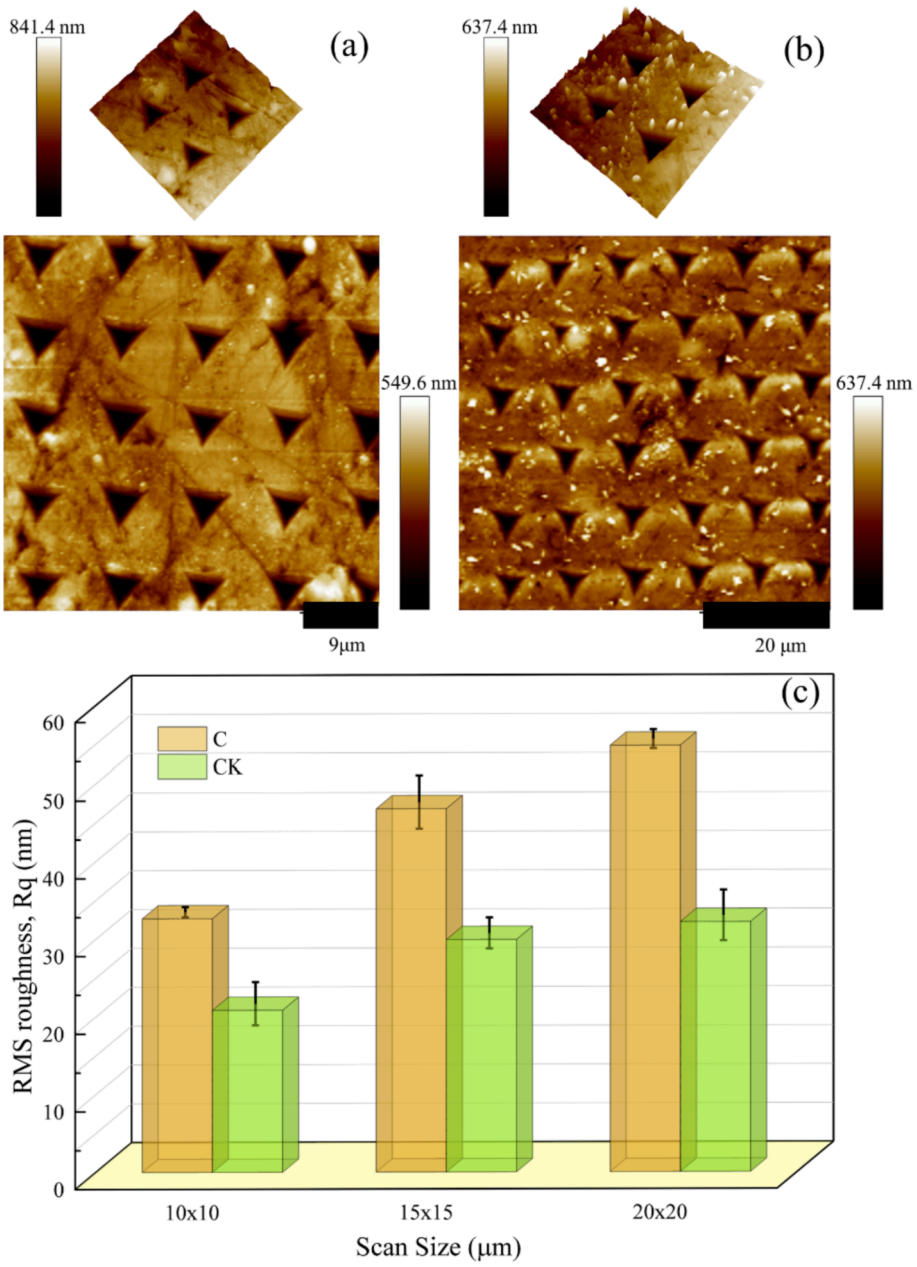

Fig. 2. (a) AFM image of indent imprints of CSA cement paste (C), (b) AFM image of indent imprints of CSA cement paste with kaolinite (CK) and (c) RMS roughness value with standard errors of CSA cement paste (C) and CSA cement paste with kaolinite (CK) for scan lengths of 10 × 10, 15 × 15 and 20 × 20 μm.

kaolinite). The images are from 60 × 60 μm areas of thin section samples which were imaged using PF-QNM mode with 512 × 512 pixel resolutions.

The AFM imaging performed on different scan sizes, e.g., 10 × 10 μm, 15 × 15 μm, and 20 × 20 μm, were analyzed digitally to determine the RMS roughness number. Fig. 2 (c) illustrates the RMS roughness and the standard error (from three analyses) of the surface topography of the thin sections. The RMS roughness value exhibits an increasing trend with increasing scan size for both sample types, which is expected due to higher variability associated with a larger scan area on the topography of such a heterogeneous material. The sample with kaolinite shows lower roughness than the sample with only CSA cement which might happen due to the smaller particle size of kaolinite occupying more surface area than the relatively larger particle size of cement in 'CK'. Overall, the sample preparation appears reasonable, leading to minimal surface roughness effects on the nanoindentation results as the indentation depth is 20-fold higher (1000 nm) than the maximum RMS roughness values, which are 55 nm and 32 nm for C and CK, respectively.

3.2. *Mapping of mechanical properties*

Representative load–displacement curves at the median reduced modulus for both 'C' and 'CK' datasets are shown in Fig. 3. The figure demonstrates a stable contact between the tip and the surface at the initial loading period. For the same designated displacement, the maximum indentation load is nearly the same for both cases. Sample 'C' shows a higher reduced modulus than 'CK' as a result of a relatively higher stiffness. In this case, the stiffness is 106.7 μN/nm for 'C' and 86.1 μN/nm for 'CK' at the maximum unloading load. The hardness values showed similar values between 'C' and CK' with a slightly larger contact area for sample 'C' (17×10^6 nm^2 vs 15.9×10^6 nm^2). Sample 'C' has a larger elastic recovery than 'CK' after the complete unloading cycle.

Fig. 4 presents the corresponding spatial mapping of the reduced

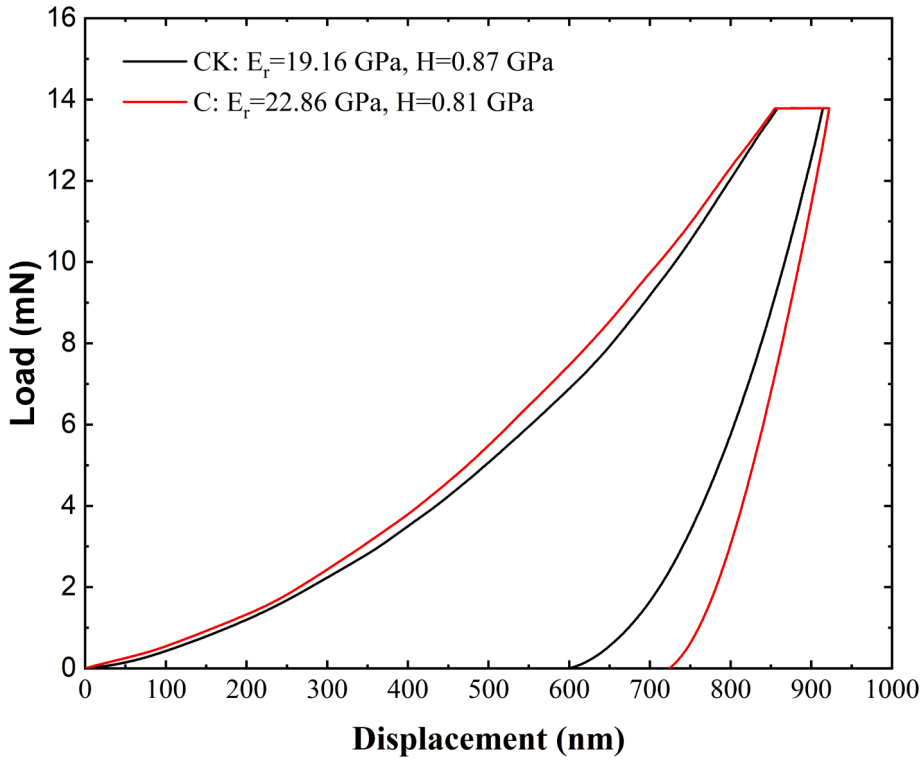

Fig. 3. Indentation load vs. displacement curve for CSA cement paste (C) and CSA cement paste with kaolinite (CK) samples.

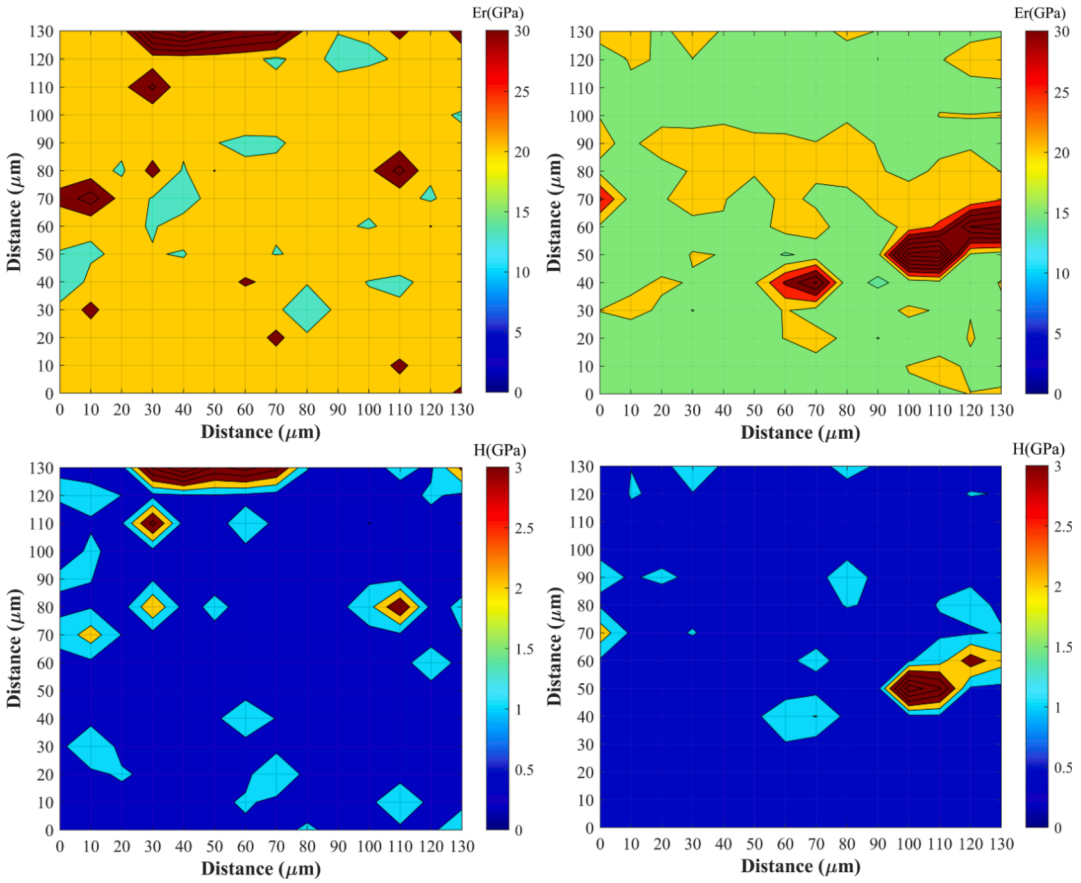

Fig. 4. Nanomechanical properties (reduced elastic modulus, E_r and hardness, H) spatial mapping via grid indentation of a sample of CSA cement paste (C) (left) and CSA cement paste with kaolinite (CK) (right). The vertical scale denotes the modulus and hardness values in GPa.

elastic modulus (E_r) and hardness (H) from 130 μm square grid indentation. The modulus and hardness maps for both cases show a similar general appearance. The mean reduced modulus for sample 'C' is somewhat higher than 'CK', which are 22.36 ± 0.08 GPa and 18.90 ± 0.06 GPa respectively. However, the hardness values are similar with a value of approximately 1.0 GPa. There are a few scattered grid points with significantly higher reduced modulus and hardness values, which we ascribe to unreacted or partially reacted hydrated phases. Modulus mapping on large-area grid provides a representative dataset and further enables analysis and identification of the major phases present in the system that underpin the strength of CSA. It is clear from the mapping of the nanomechanical data that there is a major phase that is consistent distributed throughout the sample. This hypothesis is evaluated in further detail in subsequent sections.

3.3. Statistical analysis

3.3.1. Phase identification

Nanoindentation is challenging on heterogeneous composites such as cementitious materials comprising a mixture of hydrated phases. A large indentation grid of 196 indents facilitates the extraction of representative samples for further analysis. As a first step towards statistical analysis, frequency histograms were constructed for both samples as shown in Fig. 5(a-d). Constant bin sizes of 0.3 GPa and 0.02 GPa were chosen for reduced modulus and hardness datasets, respectively, as to achieve a comprehensive statistical distribution. In this regard, a descriptive statistical analysis was executed for all the measurements. Both datasets were found to be skewed right as the mean is larger than the median in all cases. The right skewness of the datasets is also visible from the histograms with a distinct peak at around 20 GPa and 0.8 GPa for reduced modulus and hardness, respectively.

The next step was adopted as assuming the distribution as a normal distribution to identify the major phase or phases in the matrix. The theoretical probability distribution function (PDF) was estimated based on the Gaussian distribution model for a non-linear fit with the experimental data as shown in Fig. 5(a′-d′). The results of the PDF fit to the models show (Table 2) that R-square, also known as the coefficient of determination (COD), is above 0.85 for the estimated PDFs. The COD is a statistical measure to qualify the linear regression, and it establishes that there is a dominant phase for both samples, which have reduced moduli of 22.36 and 18.90 GPa, and indentation hardness of 0.78 and 0.84 GPa for samples 'C' and 'CK', respectively.

The major early hydration product, within the first 28 days, of most of the CSA cement compositions, is ettringite ($C_6A\overline{S}_3H_{32}$) which dominates the behavior of the CSA formulated matrices [32]. Being reliant on the clinker composition and available anhydrite, the dominant hydration reaction can be as follows to form crystalline ettringite ($C_6A\overline{S}_3H_{32}$) together with amorphous hydrated alumina gel (AH_3) in absence of

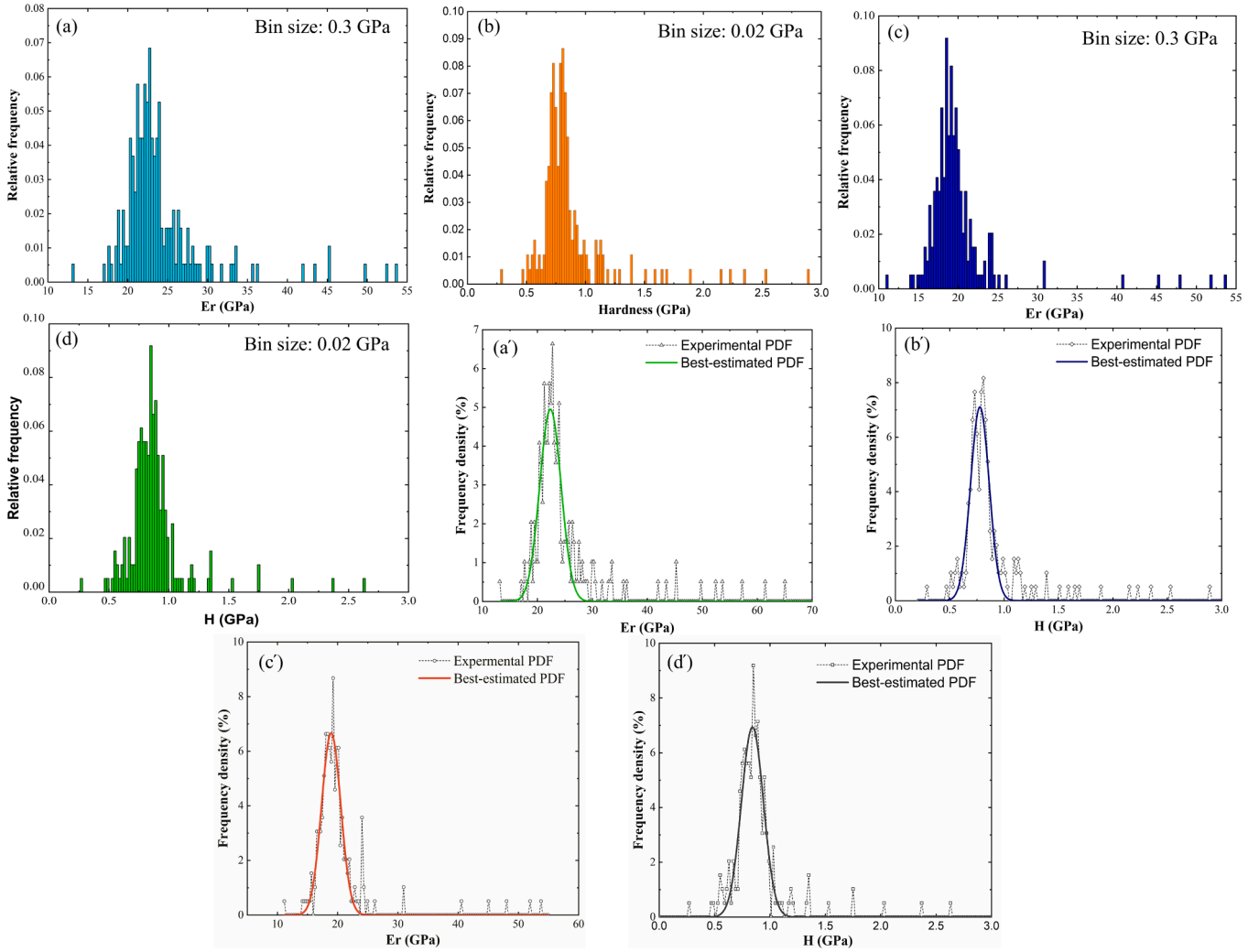

Fig. 5. Histograms of the mechanical properties: (a) reduced modulus and (b) hardness of CSA cement paste (C), (c) reduced modulus and (d) hardness of CSA cement paste with kaolinite (CK); statistical indentation analysis of w/b = 0.45 cement pastes: probability density functions (PDF) of (a′) reduced modulus and (b′) hardness of CSA cement paste (C), and, (c′) reduced modulus and (d′) hardness of CSA cement paste with kaolinite (CK).

excess calcium hydroxide (CH) [21]:

$$C_4A_3\overline{S} + 2C\overline{S}H_2 + 34H = C_6A\overline{S}_3H_{32} + 2AH_3 \quad (7)$$

(Shorthand cement chemistry notation:.$C = CaO$, $A = Al_2O_3$, $S = SiO_2$, $\overline{S} = SO_3$, $\overline{C} = CO_2$, $H = H_2O$)

The CSA cement used in the study is a ye'elimite-based cement with no lime (CH) in the clinker ingredients; therefore, equation (7) matches the scenario yielding ettringite as a major hydration product. The statistical analysis of the study indicates that the major phase has a reduced modulus of 22.36 and 18.90 GPa for samples 'C' and sample 'CK', respectively. The actual modulus of the phase, if converted from reduced modulus using equation (3), is 20.75 and 17.49 GPa for samples 'C' and 'CK', respectively,which is in good agreement with the modulus of ettringite described in previous studies [8,9,25].

3.3.2. Microstructural validation

Fig. 6A depicts the scanning electron micrograph of a representative intent on the kaolinite-infused calcium sulfoaluminate cement. Ettringite possesses needle-like morphology (Fig. 6B) and is embedded in the cement matrix. According to the XRD Rietveld analysis we observed that ettringite is the major crystalline hydration phase comprising of 29 wt% ettringite (Table S1) with respect to an Al_2O_3 internal standard in 1-day of hydration that remains almost constant over 28-days of hydration for both samples, CSA cement with and without kaolinite. Therefore, the major phase of the system has been identified as ettringite which validates the experimental and statistical hypothesis.

3.3.3. Two sample hypothesis testing

The reduced modulus vs. hardness data of sample 'C' and 'CK' (Fig. 7) approximately shows that the values are comparable, yet, it is difficult to comment on the vast datasets without any statistical hypothesis test to determine if there is any significant difference between them or if they came from two different populations. A two-sample *t*-test for an individual sample is a common approach in statistics that serves this purpose. However, the *t*-test is a parametric test to compare the mean value of the datasets which follow a normal distribution or there is equal variance between groups. On the other hand, if the data does not follow a normal distribution (skewed distribution) or it is not certain or the data size is small (<30), a non-parametric test is preferable [4]. In this study, both parametric and non-parametric hypothesis tests were performed.

A basic two-sample *t*-test was performed on the two sample groups in the study with a null hypothesis that the mean of both datasets is equal. The result of the *t*-test is shown in Table 3, which shows that the probability (p-value) value is less than the significance value, 0.05 (α), for the reduced modulus and greater than the significance value for the hardness data. That means samples 'C' and 'CK' are found to be significantly different datasets for reduced modulus measurement, but they are not significant based on the hardness data. In this study, a parametric hypothesis analysis can be erroneous as the dataset is skewed, as found in the descriptive analysis shown in Table 1.

Therefore, as a non-parametric approach, Kruskal–Wallis analysis of variance (ANOVA) was also performed for the two sets of populations of sample 'C' and 'CK'. The non-parametric approach is preferable in this case as it is applicable to any kind of dataset to categorize the rank of the samples and also to execute comparison based on the median values of the comparable groups instead of mean values. The null hypothesis was the sample 'C' and 'CK are from the same population, and the alternative hypothesis was they are from a different population. The analysis results (Table 3) show that for both the reduced modulus and hardness measurements sample 'C' and sample 'CK' are found to be significantly different. In terms of the magnitude of these differences, the mean reduced moduli were 22.36 and 18.90 GPa and the mean hardness values were 0.78 and 0.84 GPa for samples 'C' and sample 'CK', respectively.

4. Conclusions

In this study, grid nanoindentation was performed on CSA-kaolinite pastes to investigate the nanomechanical properties such as elastic modulus and hardness as well as to assess the effect of kaolinite on the properties. The observations of the study can be summarized as:

1. The load–displacement curves showed that their loading and unloading pattern was sufficiently stable to enable reliable extraction of modulus and hardness values.
2. From AFM topographic images, RMS roughness was estimated to be 55 and 32 nm for samples 'C' and 'CK', respectively. As such, the surface preparation was adequate such that the RMS of the surface roughness was 20-fold lower than the indentation depth.
3. Spatial mapping revealed that the reduced modulus and hardness values exhibit a similar trend in terms of homogeneity for both 'C' and 'CK' samples.
4. As a statistical analysis, construction of frequency histogram followed by PDF and supported by microstructural and phase analysis

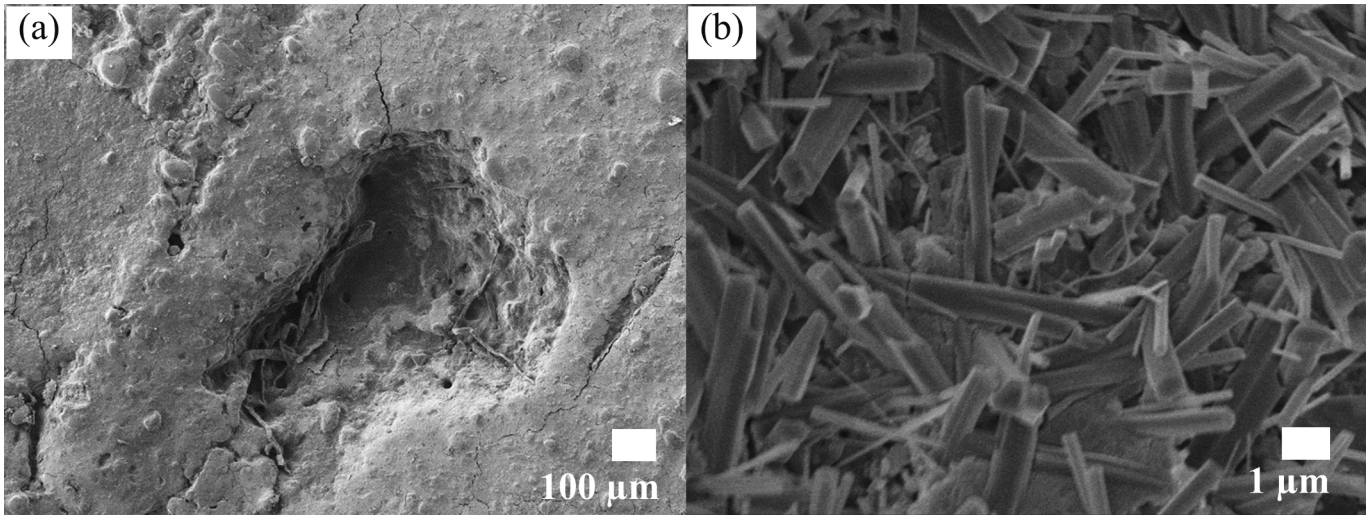

Fig. 6. Scanning electron micrographs of a) a representative indent on kaolinite-infused calcium sulfoaluminate cement; b) Ettringite-needle (major hydration phase).

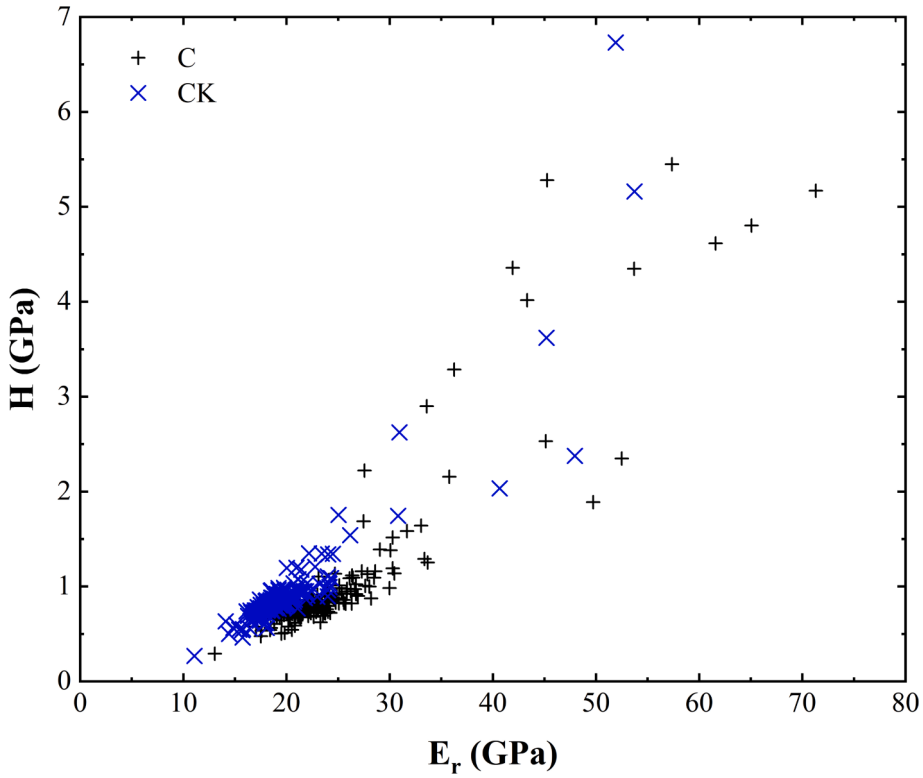

Fig. 7. Reduced modulus vs. hardness data for samples of CSA cement paste (C) and CSA cement paste with kaolinite (CK).

Table 1
Descriptive statistical analysis of the mechanical properties.

Parameters	Sample 'C'		Sample 'CK'	
	Reduced modulus, E_r	Hardness, H	Reduced modulus, E_r	Hardness, H
	(GPa)			
Mean	25.64	1.11	20.12	0.95
Standard Error	0.70	0.08	0.37	0.04
Median	22.86	0.81	19.16	0.85
Standard Deviation	9.78	1.05	5.16	0.61
Sample Variance	95.57	1.10	26.65	0.37
Kurtosis	14.7	14.86	23.26	54.96
Skewness	3.62	3.79	4.45	6.84

Table 2
Results from the statistical model fit between experimental and theoretical PDFs.

Parameters	Sample 'C'		Sample 'CK'	
	Reduced modulus, E_r	Hardness, H	Reduced modulus, E_r	Hardness, H
	(GPa)			
Mean, μ	22.36 ± 0.08	0.78 ± 0.00	18.90 ± 0.06	0.84 ± 0.00
Standard Deviation, σ	1.95 ± 0.08	0.09 ± 0.00	1.55 ± 0.06	0.099 ± 0.00
Reduced Chi-Sqr	0.21	0.13	0.28	0.12
R-Square (COD)	0.85	0.89	0.90	0.91

Table 3
Two sample hypothesis test results.

Test type	Two sample *t*-test for populations 'C' and 'CK'		
Null hypothesis, H_0	Mean 1 - Mean 2 = 0		
Alternative hypothesis, H_1	Mean 1 - Mean 2 < > 0		
Parameters	**t value**	**Probability, p-value**	**Result**
Reduced modulus, E_r (GPa)	6.95	2.30E-11	H_0 rejected - two samples significantly different
Hardness, H (GPa)	1.89	0.06	H_0 accepted - two samples are not significantly different
Test type	**Two sample Kruskal-Wallis ANOVA test for populations 'C' and 'CK'**		
Null hypothesis, H_0	The samples come from same population		
Alternative hypothesis, H_1	The samples come from different population		
Parameters	**Z value**	**Probability, p-value**	**Result**
Reduced modulus, E_r (GPa)	11.99	4.22E-33	H_0 rejected - The samples come from different population
Hardness, H (GPa)	−2.07	0.04	H_0 rejected - The samples come from different population

indicated that ettringite is the only dominant major phase for both samples.

5. The elastic modulus of ettringite is found to be 20.75 GPa and 17.49 GPa for samples 'C' and 'CK', which is concordant with previous studies.
6. From the single sample descriptive statistical analysis, the differences between the mean and median values of reduced modulus and hardness are 5 GPa and 0.16 GPa, and 3 GPa and 0.04 GPa,

respectively. Both datasets are right skewed. Hence, a non-parametric two-sample hypothesis test reveals that the measurements of these two datasets are from two different populations which are CSA paste and CSA with kaolinite pastes. The incorporation of kaolinite showed a minor impact on the mechanical properties in the CSA cement system which opens the path to utilizing *in situ* kaolinite with CSA cement as a building material ingredient which would be a sustainable innovation in the construction industry.

CRediT authorship contribution statement

Umme Zakira: Methodology, Validation, Writing – review & editing, Writing – original draft, Data curation. **Aayushi Bajpayee:** Methodology, Validation. **Matt Pharr:** Conceptualization, Visualization, Supervision, Writing – review & editing. **Sarbajit Banerjee:** Conceptualization, Visualization, Supervision, Writing – review & editing. **Bjorn Birgisson:** Conceptualization, Visualization, Supervision, Writing – review & editing.

Declaration of Competing Interest

The authors declare that they have no known competing financial interests or personal relationships that could have appeared to influence the work reported in this paper.

Acknowledgments

The authors gratefully acknowledge the Texas A&M X-grants program and J.L. “Corky” Frank/Marathon Ashland Petroleum LLC Chair funds for the support of this work, Dr. Wilson Serem for his suggestions and assistance during nano-indentation and atomic force microscopy experiments, and, Dr. Pavan Akula and Dr. Andrew Mott for their recommendations and help with sample preparation.

Appendix A. Supplementary data

Supplementary data to this article can be found online at https://doi.org/10.1016/j.conbuildmat.2022.127523.

References

[1] A. Bajpayee, M. Farahbakhsh, U. Zakira, A. Pandey, L.A. Ennab, Z. Rybkowski, M. K. Dixit, P.A. Schwab, N. Kalantar, B. Birgisson, S. Banerjee, In situ Resource Utilization and Reconfiguration of Soils Into Construction Materials for the Additive Manufacturing of Buildings, Frontiers in Materials (2020) 52, https://doi.org/10.3389/FMATS.2020.00052.
[2] L. Brown, P.G. Allison, F. Sanchez, Use of nanoindentation phase characterization and homogenization to estimate the elastic modulus of heterogeneously decalcified cement pastes, Materials and Design 142 (2018) 308–318, https://doi.org/10.1016/j.matdes.2018.01.030.
[3] J.J. Chen, L. Sorelli, M. Vandamme, F.J. Ulm, G. Chanvillard, A coupled nanoindentation/SEM-EDS study on low water/cement ratio portland cement paste: Evidence for C-S-H/Ca(OH)2 nanocomposites, Journal of the American Ceramic Society 93 (5) (2010) 1484–1493, https://doi.org/10.1111/j.1551-2916.2009.03599.x.
[4] Chin, R., & Lee, B. Y. (2008). Analysis of Data. *Principles and Practice of Clinical Trial Medicine*, 325–359. https://doi.org/10.1016/B978-0-12-373695-6.00015-6.
[5] G. Constantinides, F.J. Ulm, K. Van Vliet, On the use of nanoindentation for cementitious materials, Materials and Structures/Materiaux et Constructions 36 (257) (2003) 191–196, https://doi.org/10.1617/14020.
[6] E. Gartner, Industrially interesting approaches to “low-CO2” cements, Cement and Concrete Research 34 (9) (2004) 1489–1498, https://doi.org/10.1016/j.cemconres.2004.01.021.
[7] S. Gautham, S. Sasmal, Recent Advances in Evaluation of intrinsic mechanical properties of cementitious composites using nanoindentation technique, Construction and Building Materials 223 (2019) 883–897, https://doi.org/10.1016/J.CONBUILDMAT.2019.07.002.
[8] S. Hajilar, B. Shafei, Nano-scale investigation of elastic properties of hydrated cement paste constituents using molecular dynamics simulations, Computational Materials Science 101 (2015) 216–226, https://doi.org/10.1016/J.COMMATSCI.2014.12.006.
[9] T. Honorio, P. Guerra, A. Bourdot, Molecular simulation of the structure and elastic properties of ettringite and monosulfoaluminate, Cement and Concrete Research 135 (2020) 106126, https://doi.org/10.1016/j.cemconres.2020.106126.
[10] C. Hu, Y. Gao, Y. Zhang, Z. Li, Statistical nanoindentation technique in application to hardened cement pastes: Influences of material microstructure and analysis method, Construction and Building Materials 113 (2016) 306–316, https://doi.org/10.1016/J.CONBUILDMAT.2016.03.064.
[11] C. Hu, D. Hou, Z. Li, Micro-mechanical properties of calcium sulfoaluminate cement and the correlation with microstructures, Cement and Concrete Composites 80 (2017) 10–16, https://doi.org/10.1016/J.CEMCONCOMP.2017.02.005.
[12] C. Hu, Z. Li, A review on the mechanical properties of cement-based materials measured by nanoindentation, Construction and Building Materials 90 (2015) 80–90, https://doi.org/10.1016/j.conbuildmat.2015.05.008.
[13] C. Hu, Z. Li, Property investigation of individual phases in cementitious composites containing silica fume and fly ash, Cement and Concrete Composites 57 (2015) 17–26, https://doi.org/10.1016/j.cemconcomp.2014.11.011.
[14] J.J. Hughes, P. Trtik, Micro-mechanical properties of cement paste measured by depth-sensing nanoindentation: A preliminary correlation of physical properties with phase type, Materials Characterization 53 (2–4) (2004) 223–231, https://doi.org/10.1016/j.matchar.2004.08.014.
[15] Y. Liu, Y. Zhuge, C.W.K. Chow, A. Keegan, J. Ma, C. Hall, D. Li, P.N. Pham, J. Huang, W. Duan, L. Wang, Cementitious composites containing alum sludge ash: An investigation of microstructural features by an advanced nanoindentation technology, Construction and Building Materials 299 (2021) 124286, https://doi.org/10.1016/j.conbuildmat.2021.124286.
[16] Z. Luo, W. Li, K. Wang, S.P. Shah, Research progress in advanced nanomechanical characterization of cement-based materials, Cement and Concrete Composites 94 (May) (2018) 277–295, https://doi.org/10.1016/j.cemconcomp.2018.09.016.
[17] Y. Ma, G. Ye, J. Hu, Micro-mechanical properties of alkali-activated fly ash evaluated by nanoindentation, Construction and Building Materials 147 (2017) 407–416, https://doi.org/10.1016/J.CONBUILDMAT.2017.04.176.
[18] B. Merle, V. Maier-Kiener, T.J. Rupert, G.M. Pharr, Current trends in nanomechanical testing research, Journal of Materials Research 36 (11) (2021) 2133–2136, https://doi.org/10.1557/s43578-021-00280-9.
[19] M. Miller, C. Bobko, M. Vandamme, F.J. Ulm, Surface roughness criteria for cement paste nanoindentation, Cement and Concrete Research 38 (4) (2008) 467–476, https://doi.org/10.1016/j.cemconres.2007.11.014.
[20] J. Němeček, V. Šmilauer, L. Kopecký, Nanoindentation characteristics of alkali-activated aluminosilicate materials, Cement and Concrete Composites 33 (2) (2011) 163–170, https://doi.org/10.1016/j.cemconcomp.2010.10.005.
[21] I. Odler, Cements containing calcium sulfoaluminate. In Special inorganic cements, CRC Press, 2000, pp. 89–107.
[22] W.C. Oliver, G.M. Pharr, An improved technique for determining hardness and elastic modulus using load and displacement sensing indentation experiments, Journal of Materials Research 7 (6) (1992) 1564–1583, https://doi.org/10.1557/JMR.1992.1564.
[23] Oliver, W. C., & Pharr, G. M. (2004). Measurement of hardness and elastic modulus by instrumented indentation: Advances in understanding and refinements to methodology. www.mrs.org/publications/jmr/policy.html.
[24] L. Sorelli, G. Constantinides, F.J. Ulm, F. Toutlemonde, The nano-mechanical signature of Ultra High Performance Concrete by statistical nanoindentation techniques, Cement and Concrete Research 38 (12) (2008) 1447–1456, https://doi.org/10.1016/j.cemconres.2008.09.002.
[25] S. Speziale, F. Jiang, Z. Mao, P.J.M. Monteiro, H.R. Wenk, T.S. Duffy, F.R. Schilling, Single-crystal elastic constants of natural ettringite, Cement and Concrete Research 38 (7) (2008) 885–889, https://doi.org/10.1016/J.CEMCONRES.2008.02.004.
[26] P. Sudharshan Phani, W.C. Oliver, G.M. Pharr, Measurement of hardness and elastic modulus by load and depth sensing indentation: Improvements to the technique based on continuous stiffness measurement, Journal of Materials Research 36 (11) (2021) 2137–2153, https://doi.org/10.1557/s43578-021-00131-7.
[27] S.W. Tang, H.G. Zhu, Z.J. Li, E. Chen, H.Y. Shao, Hydration stage identification and phase transformation of calcium sulfoaluminate cement at early age, Construction and Building Materials 75 (2015) 11–18, https://doi.org/10.1016/J.CONBUILDMAT.2014.11.006.
[28] A. Telesca, M. Marroccoli, M.L. Pace, M. Tomasulo, G.L. Valenti, P.J.M. Monteiro, A hydration study of various calcium sulfoaluminate cements, Cement and Concrete Composites 53 (2014) 224–232, https://doi.org/10.1016/j.cemconcomp.2014.07.002.
[29] F.-J. Ulm, M. Vandamme, C. Bobko, J. Alberto Ortega, K. Tai, C. Ortiz, Statistical indentation techniques for hydrated nanocomposites: Concrete, bone, and shale, Journal of the American Ceramic Society 90 (9) (2007) 2677–2692, https://doi.org/10.1111/j.1551-2916.2007.02012.x.
[30] P. Wang, N. Li, L. Xu, Hydration evolution and compressive strength of calcium sulphoaluminate cement constantly cured over the temperature range of 0 to 80 °C, Cement and Concrete Research 100 (May) (2017) 203–213, https://doi.org/10.1016/j.cemconres.2017.05.025.
[31] Y. Wei, X. Gao, S. Liang, A combined SPM/NI/EDS method to quantify properties of inner and outer C-S-H in OPC and slag-blended cement pastes, Cement and

Concrete Composites 85 (2018) 56–66, https://doi.org/10.1016/j.cemconcomp.2017.09.017.
[32] F. Winnefeld, B. Lothenbach, Hydration of calcium sulfoaluminate cements - Experimental findings and thermodynamic modelling, Cement and Concrete Research 40 (8) (2010) 1239–1247, https://doi.org/10.1016/j.cemconres.2009.08.014.
[33] W. Zhu, J.J. Hughes, N. Bicanic, C.J. Pearce, Nanoindentation mapping of mechanical properties of cement paste and natural rocks, Materials Characterization 58 (11–12 SPEC. ISS.) (2007) 1189–1198, https://doi.org/10.1016/j.matchar.2007.05.018.